Transport and Communications Science Journal, Vol. 76, Issue 04 (05/2025), 638-649

Transport and Communications Science Journal

CAPACITY EVALUATION OF MIMO-OFDM HIGH-SPEED RAILWAY COMMUNICATION SYSTEMS

Do Viet Ha*

University of Transport and Communications, No 3 Cau Giay Street, Hanoi, Vietnam

ARTICLE INFO

TYPE: Research Article
Received: 15/10/2024
Revised: 14/01/2025
Accepted: 10/05/2025
Published online: 15/05/2025
https://doi.org/10.47869/tcsj.76.4.15

* *Corresponding author*
Email: dovietha@utc.edu.vn; Tel: 0906070074

Abstract. In recent years, wireless communications have been harnessed to enhance the performance, reliability, and passenger experience of high-speed railways (HSR). However, the demanding requirements of HSR systems, including high data rates, reliability, and low latency, present significant challenges for wireless communication technologies. One promising and effective approach to address these challenges is to increase system capacity through the use of multiple-input multiple-output (MIMO) techniques. Our study investigates radio wave propagation in high-speed railway environments using MRS (Mobile Relay Station). Through simulations based on a non-stationary geometry-based stochastic channel model, we evaluate the performance of MIMO techniques. Our findings reveal that while MIMO can significantly enhance system capacity, its practical gains in HSR environments are lower than predicted by theoretical models, primarily due to the significant deviations from ideal channel conditions. By analyzing numerical results on the effectiveness of MIMO configurations in enhancing system capacity, the paper determines the optimal number of transceiver antennas required to achieve the desired capacity increase without compromising design complexity. The evaluation methodology presented in this paper can serve as a valuable tool for predicting the performance of HSR communication systems before investing in costly hardware implementations.

Keywords: Capacity, HSR, MIMO, OFDM.

1. INTRODUCTION

High-speed rail (HSR) is a key indicator of a nation's development, facilitating international trade and stimulating economic growth worldwide. Renowned HSR systems like Japan's Shinkansen, Germany's Intercity-Express (ICE), France's Train à Grande Vitesse (TGV), and China's CRH operate at speeds between 300 and nearly 600 km/h. Global high-speed rail networks are expected to span millions of kilometers by 2030 [1]. Vietnam is planning to construct a 1,545-kilometer high-speed rail line from Hanoi to Ho Chi Minh City, targeting a top speed of 350 km/h and completion by 2035 [2].

Wireless technologies have advanced significantly in recent years, meeting the growing communication demands of intelligent transportation systems (ITS), particularly in the context of high-speed rail (HSR). They enhance HSR safety, efficiency, and sustainability by enabling real-time monitoring, reducing costs, expanding connectivity, and supporting advanced applications [3]. Current wireless technologies, including Wi-Fi, WiMAX, LTE, wireless sensor networks, wireless ad-hoc networks, and emerging 5G technologies, are crucial for developing intelligent transportation systems for both terrestrial and aerial vehicles. These technologies can significantly improve operation, efficiency, reliability, and passenger experience, but each communication network must be designed and configured to meet the specific requirements of the transportation system [3], [4].

Designing communication systems for high-speed rail (HSR) presents significant challenges, including high mobility and Doppler effects, seamless handover, and signal propagation issues in complex environments. These systems demand high bandwidth, low latency, effective interference management, energy efficiency, and robust security measures to ensure reliable and safe operation [5], [6]. Current research suggests that the transmission rate per train carriage, currently around 40 Mbps, could increase to 0.5-5 Gbps in the future, presenting significant challenges for existing railway wireless communication systems [5]. MIMO technology has emerged as a critical component of HSR communications due to its ability to enhance signal quality and spectral efficiency. MIMO is essential for improving the physical layer, mitigating rapidly changing fading environments, managing complex interference, and bolstering the robustness of wireless links in next-generation railway communication systems [7]. MIMO capacity increases linearly with the number of transmit and receive antennas when channel elements are uncorrelated, as in an i.i.d. Rayleigh fading model [8]. However, the strong line-of-sight (LOS) component in HSR environments limits the effectiveness of conventional MIMO techniques [6]. Additionally, the benefits of MIMO are realized only when the channel has multiple separable multipath components. To fully leverage the potential of MIMO, the MIMO channels must have a large number of significant singular values. If this condition is not met, the achievable MIMO gains may be substantially lower than theoretical values [9]. In such cases, the application of MIMO techniques must be carefully evaluated, as the additional benefits may not compensate for the increased hardware complexity and significant rise in signal processing requirements for the transceivers.

Evaluating the capacity of MIMO-OFDM systems in HSR communication systems is crucial for performance assessment. System capacity is not only a performance metric but also a fundamental parameter for system design. However, the author's survey identifies a significant gap in the literature regarding the evaluation of MIMO-OFDM system capacity for HSR. Existing studies [8], [10], [11], [12], while addressing this topic, have utilized channel models that are insufficiently accurate to fully capture the complex propagation effects in HSR

environments. To determine the MIMO system capacity for HSR, the channel model in [10] is considered with distance-dependent path loss characteristics, and the time correlation coefficient of the channel is calculated using the Bessel function. While the capacity of Cell-Free Massive MIMO-OFDM for HSR Communications in [11] is investigated by assuming a combination of line-of-sight (LOS) and a large number of statistically independent non-line-of-sight (NLOS) paths with random amplitudes. The paper [8] evaluated the capacity of a 2x2 high-altitude platform (HAP)-MIMO system for HSR communications based on the elevation angle of the incoming wave relative to the train's movement. The wireless HSR channel is modeled as Rician fading with Rician K-factors of 10dB and 30dB. The paper [12] proposed a low-complexity beam selection scheme to mitigate inter-beam ambiguity (IBA) as the train approaches the cell edge. Throughput performance was evaluated assuming small-scale fading follows a standard normal distribution. Based on the analysis of existing research, this paper will address these gaps by conducting a comprehensive study on the capacity of MIMO-OFDM systems for HSR communications, leveraging a more accurate channel model capable of capturing the intricate propagation effects inherent in HSR.

In HSR communications, unique propagation environments, such as tracks, tunnels, and viaducts, create specific radio phenomena like multiple reflections and scattering, impacting signal behaviour. For example, in tunnels, MIMO system performance can be affected by the 'Key Hole' effect and spatial correlation [7]. Additionally, extreme conditions, including high voltage near antennas, dust, rain, snow, and train vibrations, introduce impulsive noise and interference, complicating communication systems. Given the complex nature of these propagation environments, a channel model that accurately captures these characteristics and is validated by empirical data is essential. The wide-sense stationary (WSS) assumption, previously adopted to simplify HSR channel modeling [13], has been disproven by real-world measurements for HSR scenarios [14], [15]. The non-stationary nature of HSR channels significantly influences physical layer design and performance evaluation, as demonstrated by relevant measurements for HSR communication systems. Therefore, modeling HSR channels with non-stationary properties is crucial.

This paper applies the non-stationary geometry-based stochastic model (GBSM) for wideband MIMO HSR channels in rural macrocells, as proposed in [16] and further improved in [17], [18], to evaluate the capacity performance of HSR-OFDM systems. Channel model parameters are derived from measured HSR data in [19] to enhance the model's realism. To assess the effectiveness of MIMO techniques in improving HSR system performance, the capacities of SISO, SIMO, MISO, and MIMO systems with various antenna configurations are inferred from the non-stationary HSR channel model. Numerical results demonstrate that the practical MIMO gains in HSR deviate significantly from theoretical predictions. Increasing the number of antennas does not result in a linear increase in capacity. In fact, for MIMO HSR channels, capacity is even lower than that obtained in Rayleigh fading channels, often considered the worst-case scenario for wireless channels. This discrepancy can be attributed to the low multipath diversity in HSR environments, leading to correlated channels and ill-conditioned channel matrices. Consequently, using MIMO with a large number of antennas may not be the optimal solution for achieving high data rates in HSR communications, particularly for applications such as high-definition video surveillance and onboard broadband Internet.

This paper is organized as follows: Section 2 introduces the non-stationary channel model and HSR system descriptions. Section 3 focuses on the capacity computation of MIMO-OFDM

systems for HSR. Numerical and simulation results are presented and analyzed in Section 4. Finally, conclusions are drawn in Section 5.

2. SYSTEM DESCRIPTIONS AND CHANNEL MODEL

Fig. 1 depicts the HSR system with Mobile Relay Stations (MRSs) mounted on the train's surface. Consequently, the end-to-end communication between the Base Station (BS) and the Mobile Station (MS) comprises two channels: an outdoor channel and an indoor channel. This paper will investigate the outdoor channel and exploit the benefits of MIMO to improve HSR communication performance.

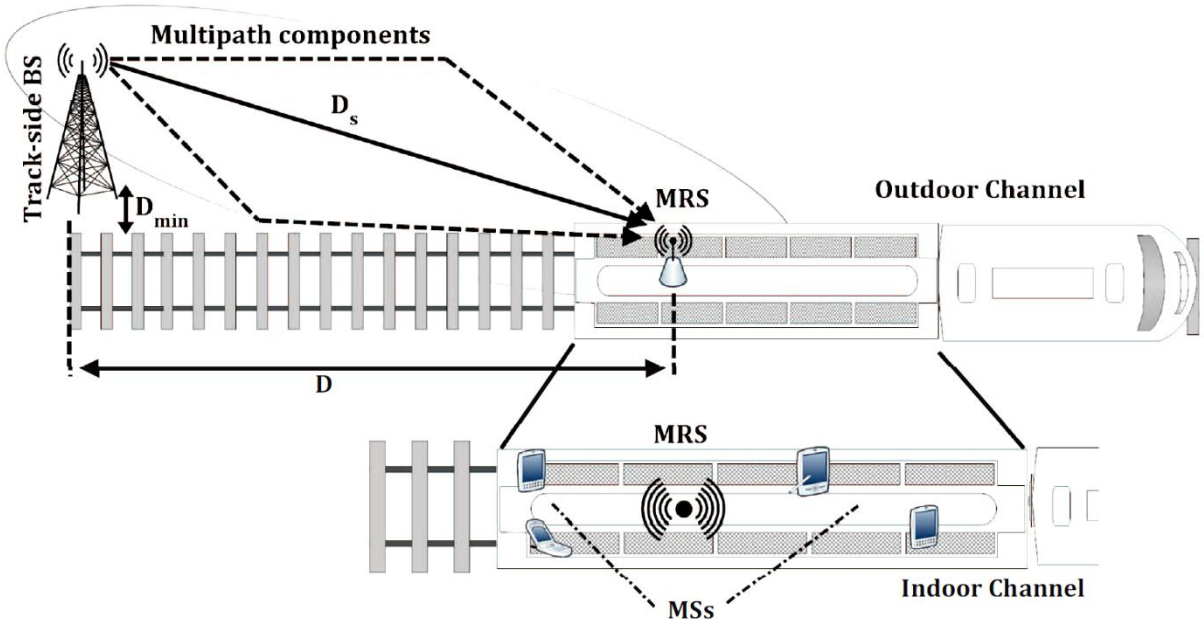

Figure 1. HSR communication system implementing MRS [16].

We consider a wideband geometry-based MIMO HSR channel model, depicted in Fig. 2, consisting of *M* transmit and *N* receive omnidirectional antennas. The channel is modeled as *I* co-focal ellipses with the BS and the train at their foci, along with a LoS component. The time-varying distance between the BS and MRS is given by $D_s(t) = \sqrt{D_{\min^2} + D^2(t)}$, where $D_{\min} = 50\text{m}$ represents the minimum distance between the BS and the track, and $D(t)$ is the projection of $D_s(t)$ onto the railway track plane. Each ellipse is assumed to have N_i scatterers. The semi-major axis of the ith ellipse is $a_i(t)$, and its semi-minor axis $b_i(t)$ can be computed by

$$b_i(t) = \sqrt{a_i^2(t) - f_s^2(t)}, \tag{1}$$

where $f_s(t) = D_s(t)/2$ represents half the distance between the two foci of the ellipses. Other geometrical parameters of the MIMO-HSR channel model are detailed in Table I.

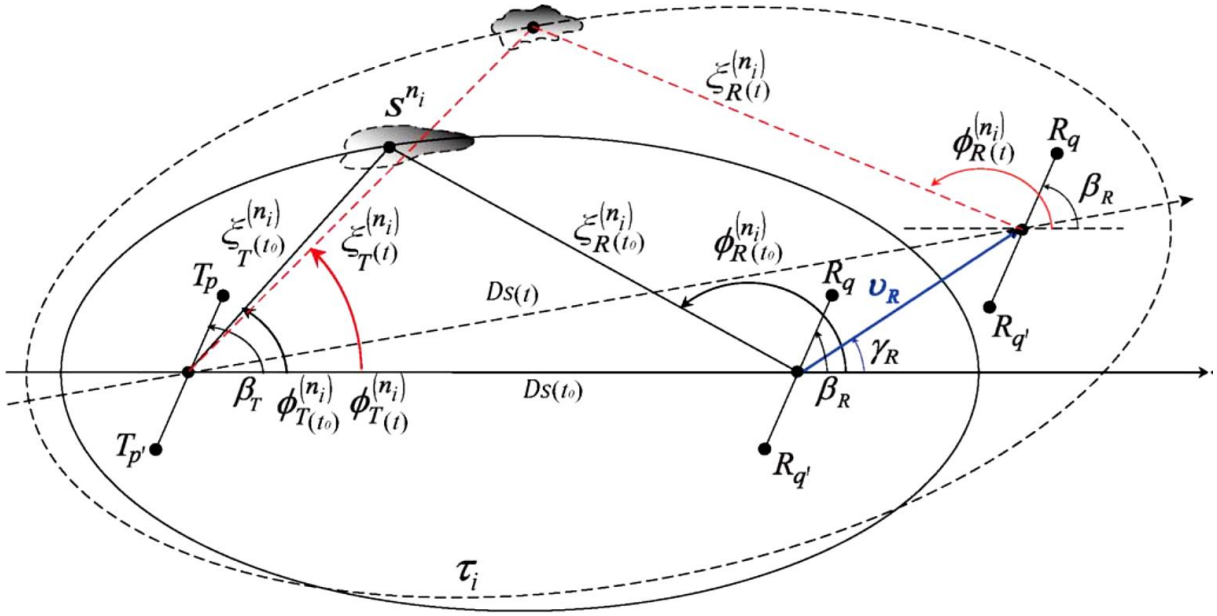

Figure 2. The geometrical ellipse model for MIMO HSR channels.

Table 1. Geometrical parameters of the MIMO-HSR channel model.

Parameters	Definition
$D_s(t)$	The time-varying distance between the BS and MRS
$f_s(t)$	Half length of the distance between the two foci of ellipses
$a_i(t),\ b_i(t)$	Semi-major and semi-minor axes of the ellipse, respectively
$v_{R,}\ \gamma_R$	MRS Speed and direction of motion, respectively
β_T, β_R	Tilt angles of the BS and MRS antenna arrays in the x-y (relative to the x-axis), respectively
$\phi_{T_p}^{LoS}(t), \phi_R^{(n_i)}(t)$	The LoS path and angles of departure (AoD) of the wave traveling from an effective scatterer $s^{(n_i)}$ to MRS, respectively
$\phi_T^{(n_i)}(t)$	AoD of the wave that impinges on the effective scatterer $s^{(n_i)}$

The time-varying channel between the BS and MRS can be characterized by the channel impulse response $h_{pq}(t,\tau)=\sum_{i=1}^{I} h_{i,pq}(t)\delta(\tau-\tau_i)$, where $h_{i,pq}(t)$ and τ_i represent the complex channel gain and propagation delay of the *i*th tap, respectively. The complex tap coefficients for the first tap (i = 1) of the T_p – R_q link is composed of a line-of-sight (LoS) component and a single-bounce (SB) component, as follow

$$h_{1,pq}=h_{1,pq}^{LoS}(t)+h_{1,pq}^{SB}(t) \tag{2}$$

where

$$h_{1,pq}^{LoS}(t)=\sqrt{\frac{K_{pq}}{K_{pq}+1}}e^{j-2\pi f_c\tau_{pq}(t)}\times e^{j2\pi f_{\max}t\cos(\phi_{T_p}^{LoS}(t)-\gamma_R)}$$

$$h_{1,pq}^{SB}(t)=\sqrt{\frac{\Omega_{1,pq}}{K_{pq}+1}}\lim_{N_1\to\infty}\sum_{n_1=1}^{N_1}\frac{1}{\sqrt{N_1}}e^{j\left(\psi_{n_1}-2\pi f_c\tau_{pq,n_1}(t)\right)}\times e^{j2\pi f_{\max}t\cos(\phi_R^{(n_1)}(t)-\gamma_R)}$$

and *p, q* denote the *p*th (*p=1,...,S)* element of the BS and *q*th (*q=1,...,U*) element of the MRS, respectively. The symbol K_{pq} represents the Ricean factor, and the average power of the *i*th tap is represented by $\Omega_{i,pq}$. The propagation time of the LoS path is given by $\tau_{pq}(t)=\xi_{pq}(t)/c$, while the propagation time of the SB path is obtained by $\tau_{pq,i}(t)=\left(\xi_{p,n_i}(t)+\xi_{n_iq}(t)\right)/c$, where *c* is the speed of light. The phase ψ_{n_i} is assumed to follow a uniform distribution over $[-\pi,\pi)$, and $f_{\max}$ represents the maximum Doppler frequency.

For other taps ($1<i\le I$), the complex tap coefficient is a sum of SB components only and obtained by

$$h_{i,pq}^{SB}(t)=h_{1,pq}^{SB}(t)=\sqrt{\Omega_{1,pq}}\lim_{N_i\to\infty}\sum_{n_1=1}^{N_i}\frac{1}{\sqrt{N_i}}e^{j\left(\psi_{n_i}-2\pi f_c\tau_{pq,n_i}(t)\right)}\times e^{j2\pi f_{\max}t\cos(\phi_R^{(n_i)}(t)-\gamma_R)} \tag{3}$$

The time-variant Angle of Arrival (AoA) of the LoS path $\phi_p^{LoS}(t)$ is expressed as

$$\phi_{T_p}^{LoS}(t)=\begin{cases}\phi_{T_p}^{LoS}(t_0)+\arccos\left(\dfrac{D_s(t_0)+v_Rt\cos\gamma_R}{D_s(t)}\right),-\pi\le\gamma_R\le 0\\ \phi_{T_p}^{LoS}(t_0)+\arccos\left(\dfrac{D_s(t_0)+v_Rt\cos\gamma_R}{D_s(t)}\right),0\le\gamma_R\le\pi\end{cases} \tag{4}$$

The distance between BS and MRS can be computed as

$$D_s(t)=\sqrt{D_s^2(t_0)+(v_Rt)^2+2D_s(t_0)v_Rt\cos\gamma_R} \tag{5}$$

Using the geometrical relations and all the angles defined in Fig.2, the mean angular value of the AoA $\mu_R^{(i)}$ is obtained as

$$\mu_R^i(t)=\begin{cases}\gamma_R-\arccos\left(\dfrac{v_Rt-\xi_R^{(n_i)}(t_0)\cos\left(\gamma_R-\mu_R^i(t_0)\right)}{\sqrt{\xi_R^{2(n_i)}(t_0)+(v_Rt)^2-2\xi_R^{(n_i)}(t_0)v_Rt\cos\left(\gamma_R-\mu_R^i(t_0)\right)}}\right), & -\pi\le\gamma_R\le 0\\ \gamma_R+\arccos\left(\dfrac{v_Rt-\xi_R^{(n_i)}(t_0)\cos\left(\gamma_R-\mu_R^i(t_0)\right)}{\sqrt{\xi_R^{2(n_i)}(t_0)+(v_Rt)^2-2\xi_R^{(n_i)}(t_0)v_Rt\cos\left(\gamma_R-\mu_R^i(t_0)\right)}}\right), & 0\le\gamma_R\le\pi\end{cases}$$

(6)

The von Mises probability density function (PDF) is defined as $f(\phi)\triangleq exp\left[kcos(\phi-\mu)\right]/\left[2\pi I_0(k)\right]$, where μ is the mean value of angle $\varphi\in[-\pi,\pi)$, $I_0(\cdot)$ is the zeroth-order modified Bessel function of the first kind, and k $(k\ge 0)$ is a positive

real-valued parameter that controls the spread of ϕ. The AoA of SB path $\phi_R^{n_i}(t)$ can be described by the Mises PDF

$$f\left(\phi_R^{n_i}\right)(t) \triangleq \frac{\exp\left[k_R^{(i)} \cos\left(\phi_R^i - \mu_R^{(i)}(t)\right)\right]}{2\pi I_0\left(k_R^{(i)}\right)}, \tag{7}$$

where $k_R^{(i)}$ is the relevant von Mises parameter that controls the spread of ϕ_R^i. Similarly, we can get $f\left(\phi_T^{(i)}\right)(t)$ with $\mu_T^{(i)}$ and $k_T^{(i)}$. The von Mises distribution for AoA modeling in HSR simulation channels has been shown to accurately represent real-world HSR channel measurements in previous studies [16-18].

Applying the modified method of equal areas (MMEA), the AoA of SB path $\left\{\phi_R^{n_i}(t)\right\}_{n_i=1}^{N_i}$ can be specified by solving the following equation

$$\frac{n_i - \frac{1}{4}}{N_i} - \int_{\mu_R^{(i)}(t_0)-\pi}^{\tilde{\phi}_R^{n_i}} f\left(\phi_R^i\right)(t_0)\, \mathrm{d}\phi_R^i = 0, \qquad n_i = 1, 2, \ldots, N_i \tag{8}$$

Combining the results of $\left\{\phi_R^{n_i}(t)\right\}_{n_i=1}^{N_i}$ obtained in Eq. (8) and the power delay profile (PDP) of HSR channel measurements, the parameters of the HSR channel model can be derived [20].

3. MIMO CAPACITY FOR HSR COMMUNICATIONS

In this section, the capacity of a MIMO-OFDM system for HSR communications is computed with *M* transmit and *N* receive antennas in a heterogeneous environment under HSR propagation scenarios.

The channel frequency response for the kth subcarrier and antenna pair (p, q) is denoted as $H_k^{(p,q)} \triangleq H\left(k/T_s\right)^{(p,q)}$, where T_s is the OFDM symbol period and $H\left(k/T_s\right)^{(p,q)}$ which is obtained by taking the Fourier transform of the channel impulse response $h_{pq}(t,\tau)$ with respect to propagation delay τ. Under these conditions, we represent the channel for the kth subcarrier by an $N \times M$ matrix H_k, which is defined as ...

$$\mathbf{H}_k = \begin{bmatrix} H_k^{(1,1)} & H_k^{(1,2)} & \ldots & H_k^{(1,M)} \\ H_k^{(2,1)} & H_k^{(2,2)} & \ldots & H_k^{(2,M)} \\ \vdots & \vdots & \ddots & \vdots \\ H_k^{(N,1)} & H_k^{(N,2)} & & H_k^{(N,M)} \end{bmatrix} \tag{9}$$

The instantaneous capacity of a specific subcarrier, assuming no channel state information is available at the transmitter, can be defined for a given channel realization as

$$C_{k,H} = \log_2\left(det\left(\mathbf{I}_N + \frac{SNR}{M}\, \mathbf{H}_k \mathbf{H}_k^H\right)\right),$$

where $\mathbf{I}_N$ denotes an $N \times N$ identity matrix and the signal-to-noise ratio SNR is given by

$$\text{SNR}=\frac{\mathbb{E}[|S_k^{(m)}|]}{\mathbb{E}[|N_k^{(n)}|]}=\frac{=2\sigma_S^2}{2\sigma_N^2} \tag{10}$$

in which S_k and N_k denote the transmitted signal and noise components of the kth subcarrier, respectively.

For an OFDM system, the overall capacity is determined by summing the capacities of N_c individual subcarriers

$$C_H = \sum_{k=0}^{N_c-1} C_{k,H} = \sum_{k=0}^{N_c-1} \log_2\left(det\left(\mathbf{I}_N + \frac{SNR}{M}\mathbf{H}_k\mathbf{H}_k^H\right)\right). \tag{11}$$

To obtain the average capacity (average over several channel realizations), the ergodic capacity must be calculated and is given by $C=\mathbb{E}_{H_k}[C_H]$.

4. NUMERICAL RESULTS

This section presents a collection of performance results related to the ergodic capacity of the MIMO-OFDM system over the wideband geometry-based HSR channel model. The number of subcarriers is assumed to be $N_c=1024$ unless specified otherwise.

A MIMO-HSR channel model was configured for system simulation based on the HSR channel measurement results in [19] for the Closer Area (CEA) scenario. The power delay profile (PDP) of the CEA scenario has three taps with propagation delays of $\tau_1=0$, $\tau_2=0.4\mu s$, and $\tau_3=1.2\ \mu s$, respectively. The PDP was used to calculate the distance between different confocal ellipses. The initial distance is $D(t_0)=135\text{m}$, $D_{\min}=50\text{m}$, and the LoS Rician factor $K_{pq}=K_{p'q'}=6\text{dB}$. The initial angle of arrival (AoA) $\mu_R^{(i)}(t0)=45°$ and the concentration parameter of the von Mises distribution $k_R^{(i)}=6$. The movement angle of the MSR speed was set to $\gamma_R=30^0$. Simulations were conducted with a vehicle speed of 360 km/h, a carrier frequency of 2.6 GHz, and a linear antenna array with varying numbers of antennas to evaluate the MIMO's impact on HSR system capacity.

Fig. 3 compares the SISO capacity of CEA scenario to AWGN and Rayleigh channels. The time-varying HSR channel results in a lower capacity than the ideal AWGN channel but higher capacity than the Rayleigh channel, a common model for worst-case wireless performance.

In contrast to the SISO results, the MIMO (2x2, 3x3, 4x4) HSR channels in the CEA scenario illustrated in Fig. 4 exhibit a different trend. For all MIMO systems, as the number of transmit and receive antennas increases, the ergodic capacity in the Rayleigh channel case is consistently better than that obtained in the actual HSR scenario. Specifically, for the 2x2 MIMO system, the CEA scenario performs almost as poorly as the Rayleigh channel. As the number of antennas increases to 3x3 and 4x4, the HSR environment with time-varying MIMO-HSR channel models exhibits even worse performance. This can be explained by the fact that in Rayleigh channels, the phase fading at each antenna is assumed to be uncorrelated [9]. In contrast, for the complex multipath environment of HSR, there can be significant correlation

between the received antennas, leading to lower capacity. In conclusion, using the Rayleigh channel to evaluate HSR MIMO systems is not reliable as the results will be overly optimistic compared to real HSR systems.

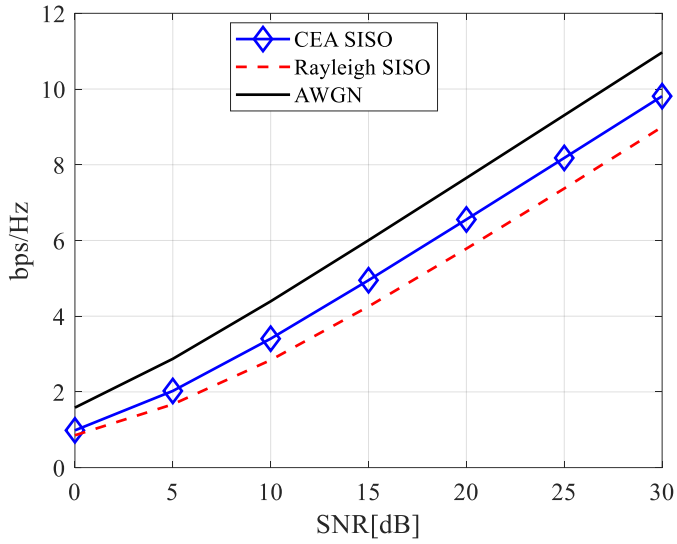

Figure 3. Comparison of SISO capacity in CEA scenario versus AWGN and Rayleigh channels.

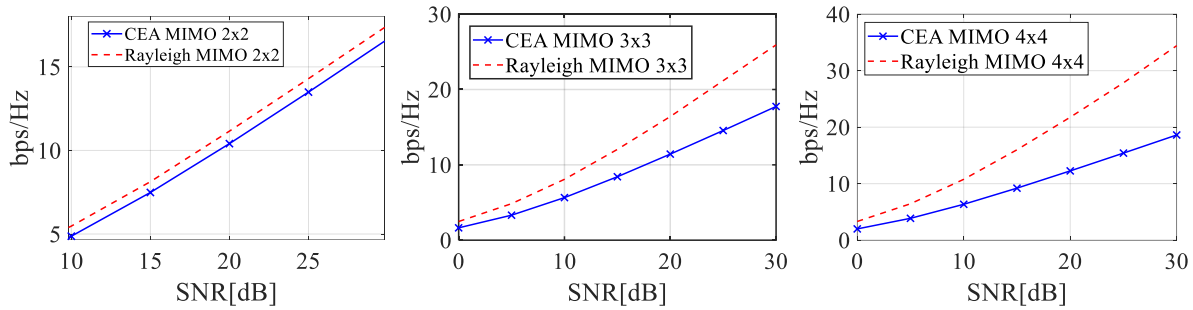

Figure 4. MIMO capacity in CEA scenario compared to Rayleigh channel.

Increasing the number of transmit and receive antennas in the HSR systems can enhance system capacity but may also increase system complexity. While MIMO configurations are often preferred, SIMO or MISO systems can also offer capacity gains in certain scenarios and may require less complex hardware. Fig.5 shows the capacity comparison for SISO, SIMO (1x4), MISO (4x1), and MIMO (4x4) configurations. The results demonstrate that the MIMO (4x4) configuration offers a significant capacity gain, especially at high SNR values. For the SIMO (4x1) configuration, increasing the number of receive antennas alone does not significantly improve capacity compared to SISO, with only about a 1bps/Hz gain for most SNR values. The MISO (4x1) configuration, however, does not yield any capacity gains compared to the SISO system. In other words, the results depicted in Fig. 5 clearly reveal that the two configurations, SIMO and MISO, fail to provide a substantial increase in system capacity. These findings highlight the effectiveness of MIMO in enhancing the capacity of HSR systems.

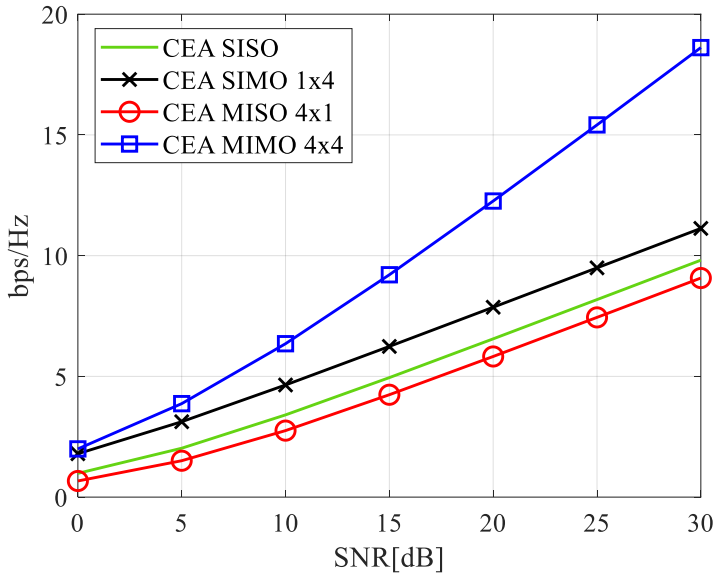

Figure 5. Capacity under CEA scenario for SISO, SIMO, MISO, and MIMO systems.

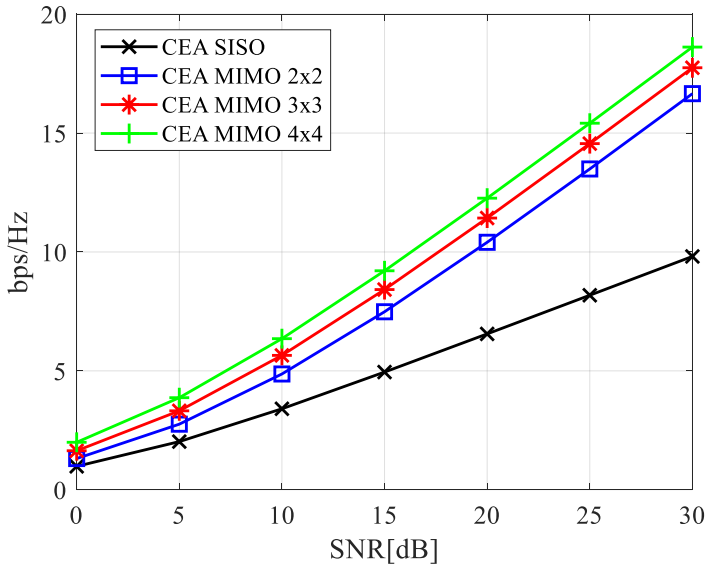

Figure 6. Capacity under CEA scenario for 2x2, 3x3, and 4x4 MIMO systems.

To investigate the impact of increasing the number of antennas on capacity in MIMO-HSR systems, the performance of different MIMO configurations HSR (2x2, 3x3, 4x4) is evaluated and the capacity results are presented in Fig. 6. The results demonstrate that the 2x2 MIMO configuration offers a significant capacity gain of approximately 6 to 7 bps/Hz compared to the SISO configuration. However, increasing the MIMO order to 3x3 and 4x4 does not yield a proportional increase in capacity. The capacity gains are marginal (approximately 1bps/Hz compared to 2x2 MIMO), while significantly increasing the complexity of signal processing and hardware implementation. This suggests that increasing the number of transmit and receive antennas in MIMO-HSR systems does not result in a linear increase in capacity.

As shown in Fig. 6, the 2x2 MIMO configuration can achieve a channel capacity of approximately 10bps/Hz at an SNR of 20dB, enabling a data rate of about 100Mbps with a 10MHz bandwidth. This is theoretically sufficient to meet the current data rate requirements of

approximately 40Mbps per train carriage as reported in [5]. However, to accommodate future demands of 0.5-5Gbps, further advancements will be necessary.

To the author's knowledge, there is limited research on the capacity of MIMO-HSR channels, with most studies using Rician fading channels or standard path loss models as presented in the introduction section. Fortunately, [18] presents measurement results showing that for a 2x2 MIMO configuration, the capacity of an HSR system can reach about 6bps/Hz when the interference-to-noise ratio (INR) is set to 10dB. The results in Fig. 6 show a channel capacity of about 10bps/Hz, which is higher than the measured result in [18]. This could be due to the additional interference (i.e. INR) introduced into the system in the measurement results, leading to a lower system performance. Furthermore, the simulated capacity reported in the paper represents the upper bound of the system's performance. Consequently, it is expected to exceed the measured capacity of a real-world HSR system. The capacity for an HSR system in [8] using a Rician fading channel model with a 2x2 MIMO configuration achieved a value of about 13bps/Hz, which is higher than the 10bps/Hz result in this paper. Thus, the results of our study using the non-stationary channel model are closer to reality.

5. CONCLUSIONS

This paper investigates the MIMO-OFDM capacity for HSR systems under CEA propagation scenario using a wideband geometry-based MIMO HSR channel model with real-world measurement data. The results demonstrate that in HSR communications, the MIMO gain is not as significant as in environments with more uncorrelated channel elements, such as Rayleigh fading channels. Nevertheless, MIMO outperforms SISO, MISO, and SIMO configurations. While the application of MIMO-OFDM to HSR is promising, increasing the number of antennas does not lead to a proportional increase in capacity. The most notable improvements are observed with the 2x2 MIMO configuration for CEA propagation scenario. Further increasing the number of antennas does not yield significant capacity gains and may increase hardware complexity and signal processing requirements. Therefore, future research should focus on techniques to enhance MIMO capacity for HSR, such as antenna configuration optimization and beamforming.

ACKNOWLEDGMENT

This research is funded by University of Transport and Communications (UTC) under grant number T2024-DT-001TĐ.

REFERENCES

[1]. V. D. Nguyen, D. V. Ha, V. V. Duong, H. A. Le, T. H. Nguyen, Joint fast time domain channel estimation with ICI cancellation for LTE-R systems, Phys. Commun., 47 (2021) 101–349. https://doi.org/10.1016/j.phycom.2021.101349

[2]. Official information about the progress of the North-South high-speed railway. https://laodong.vn/giao-thong/thong-tin-chinh-thuc-ve-tien-do-duong-sat-cao-toc-bac-nam-1402050.ldo/, (Accessed: 01 Oct. 2024)

[3]. J. Farooq, J. Soler, Radio Communication for Communications-Based Train Control (CBTC): A Tutorial and Survey, IEEE Commun. Surv. Tutor., 19 (2017) 1377–1402. https://doi.org/10.1109/COMST.2017.2661384

[4]. Q. Dong, K. Hayashi, M. Kaneko, An Optimized Link Layer Design for Communication-Based Train Control Systems Using WLAN, IEEE Access, 6 (2018) 6865–6877.

https://doi.org/10.1109/ACCESS.2017.2763173

[5]. P. Li et al., RIS-Assisted Scheduling for High-Speed Railway Secure Communications, IEEE Trans. Veh. Technol., 72 (2023) 3488–3501. https://doi.org/10.1109/TVT.2022.3218285

[6]. S. Xu, G. Zhu, B. Ai, Z. Zhong, A survey on high-speed railway communications: A radio resource management perspective, Comput. Commun., 86 (2016) 12–28. https://doi.org/10.1016/j.comcom.2016.04.003

[7]. Q. Li, J.-C. Sibel, M. Berbineau, I. Dayoub, F. Gallée, H. Bonneville, Physical Layer Enhancement for Next-Generation Railway Communication Systems, IEEE Access, 10 (2022) 83152–83175. https://doi.org/10.1109/ACCESS.2022.3192971

[8]. I. Zakia, Capacity of HAP-MIMO channels for high-speed train communications, 2017 3rd International Conference on Wireless and Telematics (ICWT), Palembang, Indonesia, (2017) 26–30. https://doi.org/10.1109/ICWT.2017.8284132

[9]. J. Guerreiro, R. Dinis, L. Campos, On the Achievable Capacity of MIMO-OFDM Systems in the CathLab Environment, Sensors, 20 (2020) 938. https://doi.org/10.3390/s20030938

[10]. Z. Liu, M. Yang, J. Cui, Y. Xiao, X. Zhang, Performance and Capacity Optimization for High Speed Railway Communications Using UAV-IRS Assisted Massive MIMO System, Electronics, 12 (2023) 2547. https://doi.org/10.3390/electronics12112547

[11]. J. Zheng, J. Zhang, E. Björnson, Z. Li, B. Ai, Cell-Free Massive MIMO-OFDM for High-Speed Train Communications, IEEE J. Sel. Areas Commun., 40 (2022) 2823–2839. https://doi.org/10.1109/JSAC.2022.3196088

[12]. J. Zhao, R. Jiang, Y. Xu, Low Complexity Beam Selection Scheme for High Speed Railway Communications, 2020 International Conference on Computing, Networking and Communications (ICNC), Big Island, HI, USA, (2020) 124–128. https://doi.org/10.1109/ICNC47757.2020.9049483

[13]. Y. Fu, C.-X. Wang, A. Ghazal, el-H. M. Aggoune, M. M. Alwakeel, Performance Investigation of Spatial Modulation Systems Under Non-Stationary Wideband High-Speed Train Channel Models, IEEE Trans. Wirel. Commun., 15 (2016) 6163–6174. https://doi.org/10.1109/TWC.2016.2580506

[14]. T. Zhou, C. Tao, L. Liu, J. Qiu, R. Sun, High-speed railway channel measurements and characterizations: a review, J. Mod. Transp., 20 (2012) 199–205. https://doi.org/10.1007/BF03325799

[15]. F. Kaltenberger et al., Broadband wireless channel measurements for high speed trains, 2015 IEEE International Conference on Communications (ICC), London, UK, (2015) 2620–2625. https://doi.org/10.1109/ICC.2015.7248720

[16]. A. Ghazal, C.-X. Wang, B. Ai, D. Yuan, H. Haas, A Nonstationary Wideband MIMO Channel Model for High-Mobility Intelligent Transportation Systems, IEEE Trans. Intell. Transp. Syst., 16 (2015) 885–897. https://doi.org/10.1109/TITS.2014.2345956

[17]. Y. Bi, J. Zhang, Q. Zhu, W. Zhang, L. Tian, P. Zhang, A Novel Non-Stationary High-Speed Train (HST) Channel Modeling and Simulation Method, IEEE Trans. Veh. Technol., 68 (2019) 82–92. https://doi.org/10.1109/TVT.2018.2882648

[18]. T. Zhou, Y. Yang, L. Liu, C. Tao, Y. Liang, A Dynamic 3-D Wideband GBSM for Cooperative Massive MIMO Channels in Intelligent High-Speed Railway Communication Systems, IEEE Trans. Wirel. Commun., 20 (2021) 2237–2250. https://doi.org/10.1109/TWC.2020.3040392

[19]. L. Liu et al., Position-Based Modeling for Wireless Channel on High-Speed Railway under a Viaduct at 2.35 GHz, IEEE J. Sel. Areas Commun., 30 (2012) 834–845. https://doi.org/10.1109/JSAC.2012.120516

[20]. Y. Fu, C.-X. Wang, A. Ghazal, el-H. M. Aggoune, M. M. Alwakeel, Performance Investigation of Spatial Modulation Systems Under Non-Stationary Wideband High-Speed Train Channel Models, IEEE Trans. Wirel. Commun., 15 (2016) 6163–6174. https://doi.org/10.1109/TWC.2016.2580506